RESEARCH ARTICLE

Filter-Based Active Damping of DAB Converter to Lower Battery Degradation in EV Fast Charging Application

NIVEDITA NAIK[1], **C. VYJAYANTHI**[1], **(Member, IEEE), AND CHIRAG MODI**[2], **(Senior Member, IEEE)**

[1]Department of Electrical and Electronics Engineering, National Institute of Technology Goa, Ponda, Goa 403401, India
[2]Department of Computer Science and Engineering, National Institute of Technology Goa, Ponda, Goa 403401, India

Corresponding author: Nivedita Naik (nivedita.naik@nitgoa.ac.in)

ABSTRACT Dual Active Bridge (DAB) converter is well suited for off-board fast Electric Vehicle Charging Stations (EVCS) and in DC microgrid-connected EVCS applications. However, proper modification in DAB converter topology is crucial for fast charging, as the charging current is very high, and any oscillations would shorten the EV battery life. As per literature, DAB converter topology integrated with a series inductor at the output for EV battery charging reduces the output current ripple by 40%. However, as per our observation, potentially unstable dynamics are introduced in the system with the inclusion of an LC filter. This affects the controller stability; hence, these dynamics must be damped using active or passive damping. Passive damping is less efficient due to the considerable losses it produces, partly induced by low-frequency noise and partly from switching-frequency noise. Also, placing the damping at the selective resonant frequency is very complex. In comparison, active damping offers selective placement and loss reduction. This paper presents the DAB converter mathematical modeling using the generalized average model (GAM) and the average output current linearization model (AOCLM). The paper presents stability analysis and proposes a novel and robust approach to control the dynamics in the current and voltage control loops during EV charging, thereby reducing battery degradation. The charge flow to the battery is controlled using Constant Current Constant Voltage (CCCV) algorithm. The proposed scheme also eliminates the need for extra sensors by selectively attenuating the oscillations at the frequency of interest. The performance of the proposed model for EV fast charging application is verified using MATLAB/Simulink and experimentally validated in a real-time simulator OPAL-RT hardware platform.

INDEX TERMS Active damping, constant current constant voltage, DAB converter, electric vehicle, notch filter, V2G.

I. INTRODUCTION

With the recent evolutions in battery technology and the growing number of Electric Vehicles (EV), the development of a fast EV charging station (EVCS) is necessary. Fast charging is a significant concern for the power grid as

The associate editor coordinating the review of this manuscript and approving it for publication was N. Prabaharan.

it demands high current in a very short span. As its impact is more pronounced during peak hours, efficient load-side management techniques are required. One possible solution is to incorporate EV and EVCS as a part of the local microgrid for vehicle-to-grid (V2G) and grid-to-vehicle (G2V) energy exchange [1], [2]. Due to their mobility and energy storage capabilities, EVs can be an ideal energy source for the microgrid system. A microgrid setup

lowers transmission losses and improves grid reliability [3]. A DC microgrid features higher efficiency, faster dynamic response, and improved current carrying capability than an AC microgrid [4], [5]. In addition, it adds more natural connect to several renewable energy sources (RESs), energy storage devices (ESDs) and EV loads [6]. All these factors result in the enhanced DC microgrid-type power structure for remotely located homes, military services, data and telecommunication hubs, EVCSs, ships, etc. [7].

Researchers are focusing on bidirectional battery power flow due to the advancements in battery technology that has enhanced life, cycle times, charging rates (C-rates), and power density [8], [9]. For DC microgrids, dc/dc converters with modular structure, isolation and bidirectional capabilities are crucial. These converters must aid with power flow back to the grid during peak hours and charge the battery when operating in the forward mode. DC level-3 and rapid EVCS delivering high current to EV can be interfaced to a DC microgrid using a dc/dc converter without any additional AC/DC converter. Multiple dc/dc converters can be stacked together within an EVCS to boost the output power for fast charging. These stacked converters can also act as solid-state transformers (SSTs) to regulate power exchange between the load and the microgrid [10].

In literature, different types of isolated bidirectional dc/dc converter (IBDC) topologies have been reported, which include three-phase push-pull [11], dual flyback [12], bidirectional-LLC resonant converter [13], dual-Cuk [14], and dual active bridge (DAB) [15]. DAB is one of the promising IBDC topologies for microgrids, energy storage applications, and EVCS due to soft-switching commutation, low device count, and high efficiency [16]- [18]. The design is ideal for applications where cost, power density, isolation, reliability, weight, and high voltage conversion factor are crucial [19], [20]. DAB's modularity and symmetrical configuration enable stacking converters for high power throughput and allow bidirectional operation [21], [22]. Mukherjee et al. [23] demonstrates that the DAB converter outperforms the LLC and other converters when operated under heavy load, resulting in 27% loss reduction compared to LLC converter.

Numerous DAB applications have been reported in the literature. Power grids have implemented SSTs built with DAB to connect different-scale microgrids at different dc voltage levels [24]. The DAB-based high-frequency power transformer for traction applications is very effective. It offers new features like HV insulation and low heat dissipation and is lighter than the traditional onboard line frequency transformers [25]. DAB has become a practical choice for onboard battery chargers for plug-in EVs. Other applications include uninterrupted power supplies (UPS), ESD interface converters, power-load emulators, and airborne wind turbines [4]. Modeling the DAB converter and designing a controller with specific steady-state and dynamic performance is crucial for all these applications.

Current research on DAB converters in EV charging includes improved strategies for zero voltage switching (ZVS) [26], [27], [28], elimination of circulating current flow [29], improvement in current carrying capacity for fast EVCS [30], high-frequency transformer saturation prevention [31], electrical design optimization [32], and cost-effective controller design [33]. Costa et al. [34] have modeled the DAB converter for EV charging by considering an inductor in series with the battery to reduce current ripples. Iyer et al. [35] have addressed the DC-link stability issues that emerge during DAB interfacing by using a virtual-resistance scheme.

To improve DAB functionality, wide-ranging research on converter structural enhancements is also in progress. In [36], a modular DAB topology is proposed by splitting one of the bridge legs and transformer, to increase control freedom for wide voltage variations in plug-in EV charging loads. Study in [17] suggests using ring-connected DAB in a multiport DC-DC converter for fast EVCS to increase power availability. A modified series-parallel resonant three-level DAB converter with ZVS operation, giving good performance in constant current constant voltage (CCCV) charging mode and short-circuited situations, is proposed in [37]. A modified DAB-converter topology with a high transformation ratio scheme is implemented in [38], to optimize conversion efficiency.

Several optimization techniques are employed in DAB control with the objective of optimizing efficiency, ZVS operation, and inductor rms-current stress. Chaurasiya et al. [39] uses particle-swarm-optimization to minimize voltage and current stress for a wide voltage off-board fast EV charger using three-level DAB. Gong et al. [27] proposed a multi-objective optimization-based modulation strategy to extend the ZVS range and achieve quasi-optimal inductor rms-current stress over the entire working range of EV chargers. In [40], a modified DAB-based charging module for fast EVCS with minimum rms current stress is proposed, wherein optimized converter parameters are obtained using genetic algorithm. Study in [41] used a multiple-duty modulation scheme to improve charging efficiency, achieve ZVS and minimize rms current stress. Haque et al. [42] proposed DAB with ZVS and reactive power (Q) control capability for an EV using mixed-modulation approach and a Q-optimization algorithm using load flow concepts. In [43], optimal duty modulation using Lagrange-multipler is proposed to realize ZVS and reduce peak-to-peak and rms current stress.

In this paper, a DAB converter and its controller are designed for EVCS, which will be connected to a DC microgrid for fast charging applications. For regulating the DAB output to control EV charging, a small signal model (SSM) is derived, and a closed-loop control system is designed. Two modeling techniques, viz., the generalized average model (GAM) and the average output current linearization model (AOCLM), are discussed, and a comparative analysis is presented in this paper.

It has been reported in the literature that the DAB converter integrated with a series inductor reduces the output current ripple by 40% [34]. However, it is observed that potentially unstable dynamics are introduced in the system with the inclusion of an LC filter. This paper proposes a novel and robust approach to damp these dynamics completely, thereby reducing the battery degradation in EVs. An active damping method is employed by cascading the DAB converter topology with a twin-T notch filter (NF). The active damping method reduces the system's complexity by modifying the controller structure and selecting appropriate control parameters, thus eliminating the requirement for an additional higher-order controller. The proposed scheme reduces the error at the resonant frequency, thereby decreasing the output voltage and current ripple and improves the dynamic performance of the entire EV charging system. It also avoids the requirement of additional sensors for measuring filter current and voltage by selective attenuation of the desired frequency. The battery is discharged by reversing the phase shift between bridges in constant current (CC) mode. CCCV algorithm is used for battery charging.

The major contributions of the paper are as follows:-

1) Design of DAB converter along with the topological modifications for reduced battery degradation during fast charging.
2) Proposed a novel and robust active damping approach using a twin-T NF to damp the potentially unstable dynamics.
3) Modeling of the DAB converter using GAM and AOCLM, along with the comparative analysis.
4) Control of EV battery charging and discharging under grid integration mode using CCCV and CC methods, respectively.

The rest of the paper is organized as follows: Section II discusses the existing DAB converter topology, it's mathematical modeling, and the controller design. Section III presents the proposed DAB converter topology cascaded with NF. The simulation results obtained using MATLAB/Simulink and the real-time simulator OPAL-RT hardware platform are presented in Section IV. Section V draws the conclusion from work.

II. EXISTING DAB TOPOLOGY, MATHEMATICAL MODELING AND CONTROLLER DESIGN FOR EV CHARGING APPLICATION

In the DAB converter, shown in Fig. 1(a), power is transferred by turning ON the MOSFET switches, which generates phase-shifted high-frequency square waves on the primary and secondary sides of the transformer. The power flows from the leading bridge to the lagging bridge, as shown in Fig. 1(b). The direction of the power flow can be reversed by reversing the phase shift. Moreover, the turning ON/OFF of the diagonal switches happen simultaneously, resulting in a square wave at the output of each bridge. The duty ratio of the primary and secondary bridge switches is set to 50%.

TABLE 1. DAB converter design parameters.

Parameter	Value	Unit	Symbol
Rated output power	10	KW	Po
Input voltage	600	V	V_1
Output voltage	380	V	V_2
Coupling inductor	20	μH	L_1
Transformer winding + Transistor ON-time resistance	1	$m\Omega$	R_1
Phase shift angle	23	degrees	ϕ
Switching frequency	100	KHz	f_s
Output capacitor	10	μF	C_2
Snubber capacitor 1°	1	nF	Cs_1
Snubber capacitor 2°	1.3	nF	Cs_2
Output inductor	46	μH	L_2
Turns ratio	1:0.633	-	1:n
Battery resistance	11	$m\Omega$	R_0
Dead time	319	nsec	T_d

The most critical factor in designing the power stage of DAB include the choice of coupling inductor, switching frequency, phase shift, design of transformer magnetics, and desired ZVS range. Most of these design factors are interdependent. For instance, the phase shift of the converter's operation at the target power level depends directly on the maximum power transfer, which in turn depends on the coupling inductor selection. Switching frequency (f_s) decides the efficiency and power density of the converter. Using SiC MOSFETs in the power stage allows the converter to operate at high f_s. Higher f_s makes it possible to use smaller magnetics, which improves the thermal solution and raises the converter's power density. Therefore, the allowable heat sink solution and transformer size are traded off when selecting f_s for a specific target efficiency. Moreover, if the chosen MOSFET has high output capacitance, setting high f_s results in significant switching losses at light loads, thereby reducing the efficiency. Thus, the selection of f_s significantly impacts the implementation of the control loop bandwidth. The auxiliary inductor (L_1) manages the power transfer, which directly adds to the transformer inductance in DAB. The LC filter connected across the battery terminal minimizes the ripples in the charging/discharging current. Considering all these factors, we have designed the DAB converter as per the specifications tabulated in Table 1. The mathematical modelling is presented below to achieve the desired specifications for the DAB converter design.

A. MATHEMATICAL MODELING OF THE EXISTING DAB TOPOLOGY

A mathematical model of the existing DAB topology is derived using GAM and AOCLM techniques. It is assumed that the effect of equivalent series resistance (ESR) of the output capacitor is zero. Note that GAM is a complex modeling technique and provides a 4th order model. However, it offers additional insights into the dynamics of the converter.
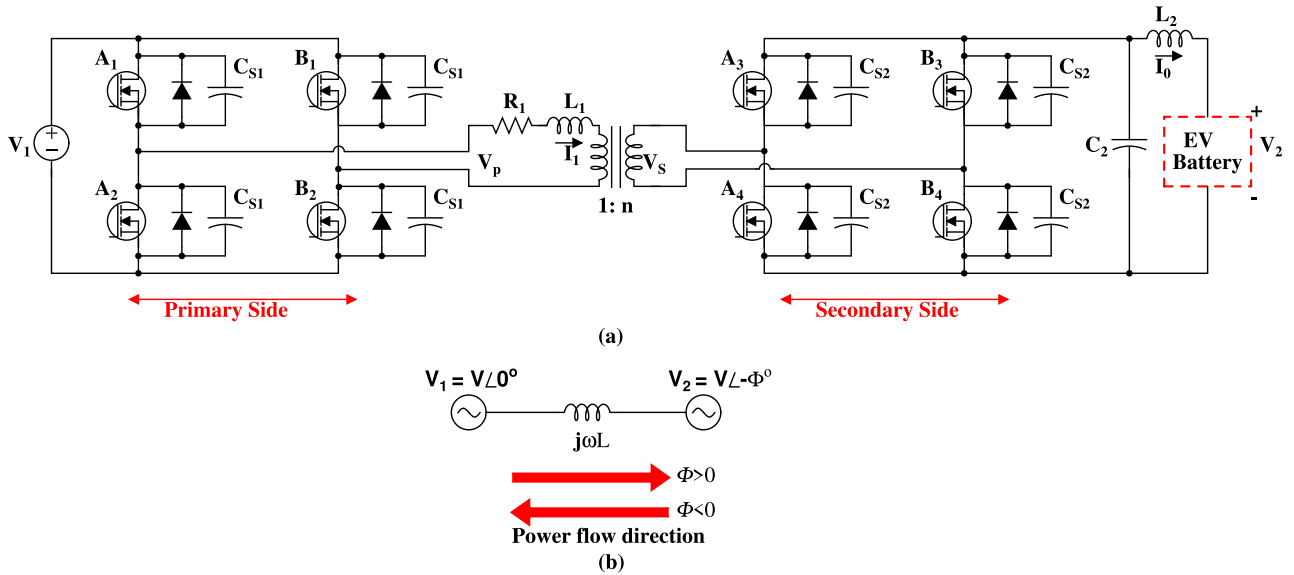
FIGURE 1. (a) DAB converter conventional topology (b) Operating principle.

On the contrary, the AOCLM model is simple and provides a 1st order model. It is developed by ignoring the non-linear terms of the coupling inductor current. A comparative analysis of both these techniques is presented to evaluate the performance of the DAB converter for EV battery load.

1) GENERALIZED AVERAGE MODELING (GAM)

GAM considers time-dependent expansion of the Fourier series [44]. It is based on the fact that approximation of any arbitrary signal $y(\tau)$ over the period $(t - T_s, t)$ to some random precision can be carried out using Fourier series, represented as:

$$y(\tau) = y(t - T_s + s) = \sum_k \langle y \rangle_k(t) \, e^{jk\omega_s(t-T_s+s)} \quad (1)$$

where, $s \in (0, T_s]$, $\omega_s = 2\pi/T_s$, $\tau = t - T_s + s$. Also, $\langle y \rangle_k(t)$ is a complex Fourier or index-k coefficient [45], which is a function of time, expressed as:

$$\langle y \rangle_k(t) = \frac{1}{T_s} \int_0^{T_s} y(t - T_s + s) \, e^{-jk\omega_s(t-T_s+s)} ds \quad (2)$$

Consider, a switched converter model with the switching function $u(t)$ having period T_s, described by

$$\frac{d}{dt} y(t) = f(y(t), u(t)) \quad (3)$$

GAM is obtained by computing the average value of the above differential equation. The Fourier coefficient for the state variable is given by,

$$\left\langle \frac{d}{dt} y \right\rangle_k = \langle f(y, u) \rangle_k \quad (4)$$

GAM retains more terms of Fourier series coefficients, which provide more insights into the converter dynamics. For
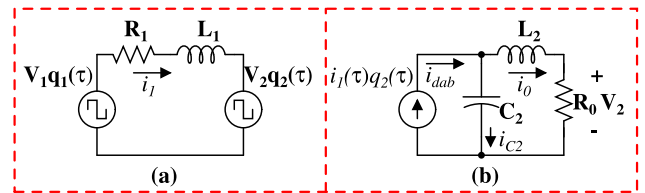

FIGURE 2. DAB equivalent circuit with GAM depicting the (a) Primary side and (b) Secondary side of the converter.

simplicity, the index 0 coefficient is used for the states with slowly varying behavior and index 1 for those with sinusoidal behavior. With only the index 0 terms, the modeling gets reduced to conventional state-space averaging. The ripple component's impact on the average values can be shown by the index 1 term of the switching function and state variables [46], [47].

The equivalent circuit of the DAB converter for GAM is shown in Fig. 2. The voltage across the primary and secondary bridge depends on the voltages V_1 and V_2 as well as the switching functions $q_1(\tau)$ and $q_2(\tau)$, respectively. Considering the capacitor voltage and current through the inductors (L_1 and L_2) as the state variables and applying Kirchhoff's law, we obtain:

$$\frac{d}{dt} i_1(\tau) = \frac{V_1}{L_1} q_1(\tau) - \frac{R_1}{L_1} i_1(\tau) - \frac{V_2}{L_1} q_2(\tau) \quad (5)$$

$$\frac{d}{dt} V_2(\tau) = \frac{i_1(\tau) q_2(\tau)}{C_2} - \frac{i_0(\tau)}{C_2} \quad (6)$$

$$\frac{d}{dt} i_0(\tau) = \frac{V_2(\tau)}{L_2} - \frac{R_0 i_0(\tau)}{L_2} \quad (7)$$

Equations (5) - (7) are non-linear as well as time-varying. Thus, averaging is used to achieve a linear and time-invariant

model. The switching functions $q_1(\tau)$ and $q_2(\tau)$ are given by:

$$q_1(\tau) = \begin{cases} +1, & 0 \le \tau < \dfrac{T_s}{2}, \\ -1, & \dfrac{T_s}{2} \le \tau < Ts \end{cases} \quad (8)$$

$$q_2(\tau) = \begin{cases} +1, & \dfrac{dT_s}{2} \le \tau < \dfrac{T_s}{2} + \dfrac{dT_s}{2} \\ -1, & \dfrac{T_s}{2} + \dfrac{dT_s}{2} \le \tau < T_s \end{cases} \quad (9)$$

where $T_s = 1/f_s$ is the switching period, $d = \phi/\pi$, and $\tau = t - T_s + s$.

We use single-phase shift modulation:

1) The voltage at the transformer primary, V_p, has two states: a) $+V_1 : A_1, B_2$ ON, b) $-V_1 : A_2, B_1$ ON. Thus, V_p can be given by,

$$V_p(\tau) = q_1(\tau)V_1(\tau) \quad (10)$$

2) Similarly, the voltage at the transformer secondary, V_s, has two states: a) $+V_2 : A_3, B_4$ ON, b) $-V_2 : A_4, B_3$ ON. Hence, V_s can be given by,

$$V_s(\tau) = q_2(\tau)V_2(\tau) \quad (11)$$

The Fourier coefficients of switching functions $q_1(\tau)$ and $q_2(\tau)$ are computed by considering 50% duty ratio, as given below:

$$\langle q_1 \rangle_0 = \langle q_2 \rangle_0 = 0 \quad (12)$$

$$\langle q_1 \rangle_1^R = 0 \quad (13)$$

$$\langle q_1 \rangle_1^I = \frac{-2}{\pi} \quad (14)$$

$$\langle q_2 \rangle_1^R = \frac{-2}{\pi} Sin(d\pi) \quad (15)$$

$$\langle q_2 \rangle_1^I = \frac{-2}{\pi} Cos(d\pi) \quad (16)$$

By applying the generalized averaging to (5),(6), and (7), and utilizing the complex conjugate, differentiation, and convolution properties of Fourier series, as well as substituting the Fourier coefficients of the switching functions obtained in (12)-(16), the index 0 and 1 averages are calculated, resulting in the derivation of a large signal generalized average model as presented in (17).

$$\begin{bmatrix} i_{1_{1R}} \\ i_{1_{1I}} \\ v_{2_0} \\ i_{0_0} \end{bmatrix} = \begin{bmatrix} \frac{-R_1}{L_1} & \omega_s & \frac{2SinD\pi}{\pi L_1} & 0 \\ -\omega_s & \frac{-R_1}{L_1} & \frac{2CosD\pi}{\pi L1} & 0 \\ \frac{-4SinD\pi}{\pi C_2} & \frac{-4CosD\pi}{\pi C_2} & 0 & \frac{-1}{C_2} \\ 0 & 0 & \frac{1}{L_2} & \frac{-R_0}{L_2} \end{bmatrix} \begin{bmatrix} i_{1_1}^R \\ i_{1_1}^I \\ v_{2_0} \\ i_{0_0} \end{bmatrix}$$
$$+ \begin{bmatrix} 0 \\ \frac{-2}{\pi L_1} \\ 0 \\ 0 \end{bmatrix} V_1 \quad (17)$$

A Small Signal Model (SSM) representing the converter's dynamic response towards the deviations in the control signal is derived for designing the controller and conducting a stability study of the closed-loop system.

In the event of perturbations in the state variable, the magnitude of $i_{1_{1R}}, i_{1_{1I}}, v_{2_0}$ and i_{0_0} will deviate from the steady state values. By perturbing the variable of interest followed by linearization, the steady state and small signal variables from the large signal model can be extracted to produce the SSM. In SSM, the state variables in capital letter refer to the steady state, and the perturbations are identified by including '^' on top. We assume perturbations in the input voltage V_1 to be zero. We use sine and cosine small angle approximations, i.e. $Cos(\pi \hat{d}) = 1$ and $Sin(\pi \hat{d}) = \pi \hat{d}$, to obtain the linearized equations as follow:-

$$Sin\pi(D + \hat{d}) = Sin\pi D + \pi \hat{d} Cos\pi D \quad (18)$$
$$Cos\pi(D + \hat{d}) = Cos\pi D - \pi \hat{d} Sin\pi D \quad (19)$$

$$\begin{bmatrix} \hat{i}_{1_1}^R \\ \hat{i}_{1_1}^I \\ \hat{v_{2_0}} \\ \hat{i_{0_0}} \end{bmatrix} = \begin{bmatrix} \frac{-R_1}{L_1} & \omega_s & \frac{2SinD\pi}{\pi L_1} & 0 \\ -\omega_s & \frac{-R_1}{L_1} & \frac{2CosD\pi}{\pi L1} & 0 \\ \frac{-4SinD\pi}{\pi C_2} & \frac{-4CosD\pi}{\pi C_2} & 0 & \frac{-1}{C_2} \\ 0 & 0 & \frac{1}{L_2} & \frac{-R_0}{L_2} \end{bmatrix} \begin{bmatrix} \hat{i}_{1_1}^R \\ \hat{i}_{1_1}^I \\ \hat{v_{2_0}} \\ \hat{i_{0_0}} \end{bmatrix}$$

$$+ \begin{bmatrix} \frac{2CosD\pi}{L_1} V_{2_0} \\ \frac{-2SinD\pi}{L_1} V_{2_0} \\ \frac{-4}{C_2}((CosD\pi)I_{1_1}^R - (CosD\pi)I_{1_1}^I) \\ 0 \end{bmatrix} \hat{d} \quad (20)$$

Using SSM as shown in (20), the relation between the variation of phase shift for the designed DAB converter to the variation in requisite state variables, i.e., battery voltage δV_2, and current δi_o, is derived.

2) AVERAGE OUTPUT CURRENT LINEARIZATION MODEL (AOCLM)

The AOCLM is developed by ignoring the non-linear terms of the coupling inductor current. The equivalent circuit for the AOCLM is shown in Fig. 3. The power output of DAB depends on the phase shift angle, ϕ, given by:

$$P = \frac{nV_1V_2\phi(1 - \frac{\phi}{\pi})}{2\pi^2 L_1 f_s} \quad (21)$$

From (21), it can be concluded that the relation between i_{dab} and ϕ is non-linear. Average output current of the DAB (i_{dab}) is given by,

$$i_{dab} = \frac{V_1\phi(1 - \frac{\phi}{\pi})}{2n\pi L_1 f_s} \quad (22)$$

By perturbing and linearizing (22), we obtain

$$\triangle i_{dab}(t) = \frac{V_1}{2n\pi L_1 f_s} \left(1 - \frac{2\phi}{\pi}\right) \triangle \phi(t) \quad (23)$$

Applying KCL to the equivalent circuit in Fig. 3 and substituting in (23), the output-voltage to phase-shift transfer function (TF) becomes:

$$\frac{V_2(s)}{\phi(s)} = \frac{V_1}{2n\pi L_1 f_s} \left(1 - \frac{2\phi}{\pi}\right) \frac{sL_2 + R_0}{s^2 C_2 L_2 + sC_2 R_0 + 1} \quad (24)$$
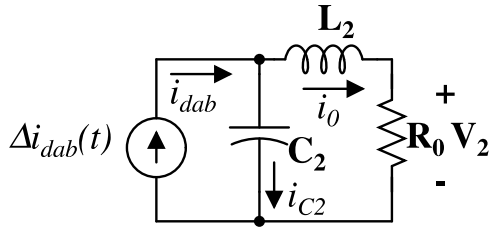
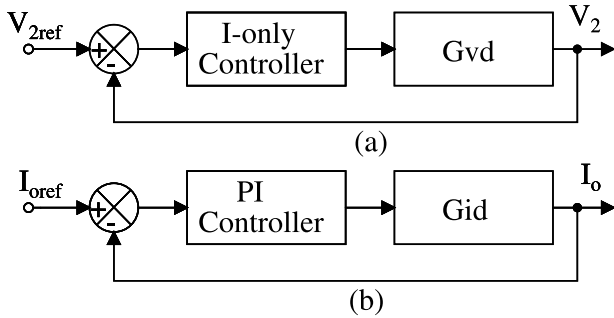**FIGURE 3.** DAB equivalent circuit with AOCLM.

FIGURE 4. Closed-loop model of DAB for (a) Current control (b) Voltage control.

Similarly, output-current to phase-shift TF is calculated as:

$$\frac{i_0(s)}{\phi(s)} = \frac{V_1}{2n\pi L_1 f_s}\left(1 - \frac{2\phi}{\pi}\right)\frac{1}{s^2 C_2 L_2 + s C_2 R_0 + 1} \quad (25)$$

B. CONTROLLER DESIGN AND STABILITY ANALYSIS

To improve the performance and stability of the system, a closed-loop model consisting of the PID controller and the DAB model for the voltage/current control is developed, as shown in Fig. 4. Equations (26) and (27) represent the output-current to phase-shift and output-voltage to phase-shift TF, respectively, obtained using GAM. Here, d represents the phase shift between the two bridges.

$$G_{id,cGAM}$$
$$= \frac{3.25 \times 10^{10}s^2 + 3.25 \times 10^{12}s + 7.9 \times 10^{22}}{s^4 + 339s^3 + 4 \times 10^{11}s^2 + 9.6 \times 10^{13}s + 8.6 \times 10^{20}} \quad (26)$$

$$G_{vd,cGAM}$$
$$= \frac{1.5 \times 10^6 s^3 + 5 \times 10^8 s^2 + 3.6 \times 10^{18}s + 8.7 \times 10^{20}}{s^4 + 339s^3 + 4 \times 10^{11}s^2 + 9.6 \times 10^{13}s + 8.6 \times 10^{20}} \quad (27)$$

Similarly, TF using the AOCLM method is obtained by substituting parameters from Table 1 in (24) and (25), as below:

$$G_{id,cAOCLM} = \frac{56.54}{4.6 \times 10^{-10}s^2 + 1.1 \times 10^{-7}s + 1} \quad (28)$$

$$G_{vd,cAOCLM} = \frac{0.002601\,s + 0.622}{4.6 \times 10^{-10}s^2 + 1.1 \times 10^{-7}s + 1} \quad (29)$$

The PID controller is tuned to obtain minimum error between the desired and actual parameters. The obtained parameters

TABLE 2. PID controller parameters.

Modeling Type	Controller Type	Parameter
GAM	Current Control	$K_P = 8.49 \times 10^{-9}$
		$K_I = 0.0761$
		$K_D = 2.37 \times 10^{-16}$
	Voltage Control	$K_I = 0.198$
AOLCM	Current Control	$K_P = 1.36 \times 10^{-8}$
		$K_I = 0.124$
		$K_D = 3.75 \times 10^{-16}$
	Voltage Control	$K_I = 0.322$
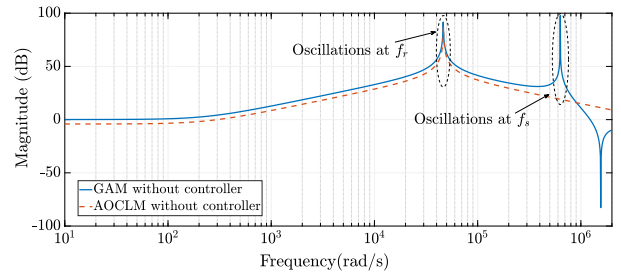
(a)
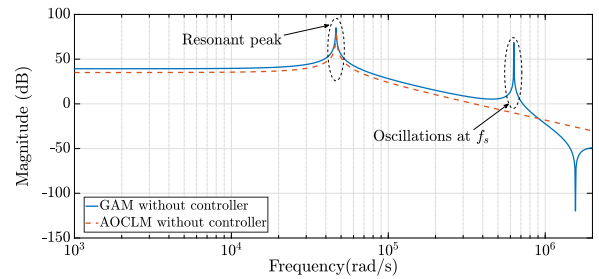
(b)

FIGURE 5. Bode magnitude plot using GAM and AOCLM for (a) Voltage to phase-shift and (b) Current to phase-shift TF without considering controller.

are shown in Table 2. The Bode magnitude plot of the open-loop TF using GAM and AOCLM technique without considering the controller is shown in Fig. 5a and Fig. 5b and with the controller is shown in Fig. 6a and Fig. 6b for voltage and current control mode respectively. The Bode plot indicates the presence of overshoot in both the voltage and current control modes of GAM and AOCLM. The GAM produces oscillations at the resonant frequency and switching frequency, while AOCLM produces oscillations only at the resonant frequency.

Both the GAM and AOCLM with controller exhibit a resonant peak caused by the presence of a pole at the origin in the open-loop TF of the system, resulting in increased rise time (t_r). The peak in switching frequency can be linked to the existence of zeros along the imaginary axis in the GAM. Thus, charging the battery at high currents and voltages, particularly during fast charging, will significantly reduce its lifespan. Compared to GAM, AOCLM presents a simple, more accurate and second-order model, and thus we have chosen AOCLM for the voltage and current controller design.
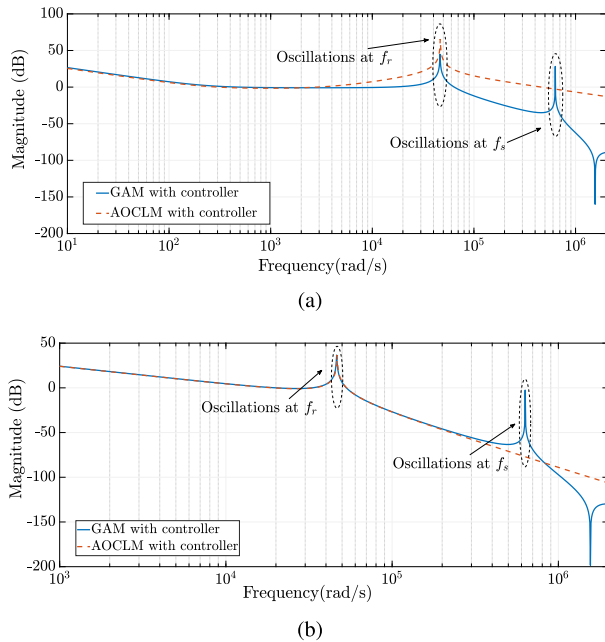
FIGURE 6. Bode magnitude plot using GAM and AOCLM for (a) Voltage to phase-shift and (b) Current to phase-shift TF considering controller.

III. PROPOSED DAB TOPOLOGY, MATHEMATICAL MODELING AND CONTROLLER DESIGN FOR EV CHARGING APPLICATION

We analysed that the LC filter connected across the DAB converter output for lowering the ripple content induces unstable dynamics in the system. These unstable dynamics occurring at the switching frequency and LC filter resonant frequency can significantly result in large voltage ripples at the output, which can cause problems in sensitive loads and reduce system efficiency. Overshoot can lead to instability in the control loop, causing excessive oscillations and reduction of the system's overall stability. It can trigger the over-current protection, causing the converter to shut down or reduce its output power, leading to power interruptions or reductions. The overshoot can cause the battery voltage to go above the rated maximum voltage, which can cause permanent damage and reduce its lifespan. Additionally, it can result in a high current surge in the battery, causing thermal stress on the cells, overheating, and further damage. Also, it may cause excessive battery discharge, which can reduce the battery's available capacity. In addition, overshoot can also lead to poor regulation of the battery voltage, which can cause instabilities in the system and affect the performance of the EV. Hence, minimising overshoot in the DAB converter is crucial to avoid damage to the battery and guarantee optimal system performance.

A. PROPOSED DAB TOPOLOGY AND MATHEMATICAL MODELING

The frequency at which the system exhibits unstable dynamics is found to be equal to the resonant frequency of the output LC filter, given by $f_r = 1/(2\pi\sqrt{L_2 C_2})$. Substituting

for L_2 and C_2, gives f_r equal to 46625 rad/sec. These oscillations can be damped using either active or passive damping. Compared to passive, active damping offers a selective placement and loss reduction. Passive damping is less efficient due to its considerable losses, partly induced by low-frequency noise and partly from switching frequency noise. The passive damping solution is less effective as placing the damping at the selective resonant frequency is very complex. Active damping, on the other hand, involves modification of the structure of the controller or changing the control parameters to achieve desired gain margin (GM) and phase margin (PM) around the appropriate resonant frequency. Moreover, to carry out active damping, the sampling rate or the control frequency must be two times the resonance frequency to control the unstable dynamics effectively.

In this paper, we have proposed a robust and straightforward method for EV battery charging using a DAB converter that uses active damping to eliminate unstable dynamics. Here, the existing DAB topology is modified by cascading a twin-T notch filter, with parameters $R = 214\ \Omega$ and $C = 0.1\ \mu F$ at the output, as shown in Fig. 7. The designed filter can be connected directly across the converter. The effective impedance Z_0 of the cascade connection of battery and filter is given by (30), as shown at the bottom of the next page.

The system dynamics as a whole, including active damping, are considered while tuning the PI controller. The GM and PM are obtained for the open-loop system to determine system stability. The new transfer functions considering filter impedance are derived using the AOCLM method. The output-voltage to phase-shift ($G_{vd,p}$) and output-current to phase-shift ($G_{id,p}$) TF becomes (31) and (32), as shown at the bottom of the next page.

The GM and PM are obtained for the open-loop system to determine system stability. GM very close to unity and PM nearing zero implies the system has oscillatory behaviour, while large GM or PM indicates a sluggish response. A balance between both is usually set up to obtain good relative stability. However, as the battery load is dynamic and any overshoot will result in the degradation of the battery, slow response time and high PM are selected. Accordingly, after choosing the performance parameters, the PID controller is tuned so that the error between the desired and actual parameters approaches zero. The gain cross-over frequency (ω_{gc}) sets the control bandwidth. High ω_{gc} increases the response time at the cost of reduced stability. Considering this, we have chosen PM=90° and ω_{gc} is set to 7 rad/sec and 0.2 rad/sec for the current and voltage controller, respectively. The modified PID controller structure is shown in Fig. 8, and the performance parameters are specified in Table 3.

Theoretically, the system's stability can be improved by reducing the proportional gain of the PID controller, but at the cost of reduced bandwidth [48]. The proposed active damping method not only achieves resonance damping but also improves the proportional gain of the PID controller,
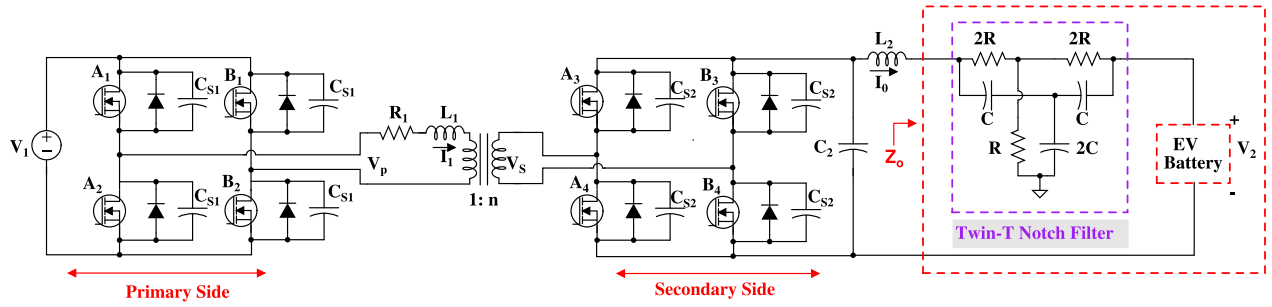
FIGURE 7. Proposed DAB converter topology considering twin-T notch filter in cascade.

TABLE 3. PID controller parameters with active damping.

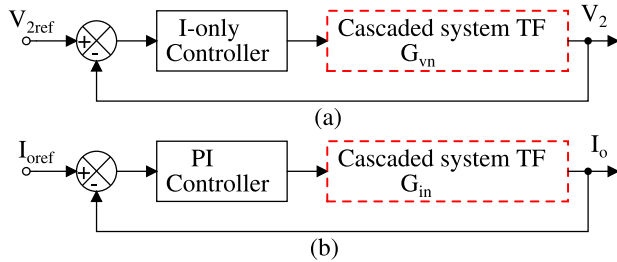| Controller Type	Parameter
Current Control	$K_P = 5.28 \times 10^{-4}$
	$K_I = 0.124$
Voltage Control	$K_I = 8.28 \times 10^{-6}$

FIGURE 8. Controller design for the cascaded system in (a) Voltage control mode (b) Current control mode.

thus satisfying the requirement of bandwidth. Moreover, the proposed method also aids in the improvement of the robustness margin by handling parameter uncertainties and improving the system stability. The proposed scheme for design and implementation of filter-based active damping of the DAB converter for EV fast charging is demonstrated in Algorithm 1.

The proposed system is used for charging the Li-ion battery. Li-ion is preferred in most EVs owing to the high energy density requirement during driving. We have used CCCV algorithm [49] for the battery charging. In CCCV at low SoC, battery charging occurs in the constant current mode, wherein the charging process begins with a constant current value. This value is set based on the desired C-rate and

---

Algorithm 1 Scheme for Design and Active Damping of the DAB Converter for EV Fast Charging

1) Read input voltage (V_1), output voltage (V_2), EV battery rated capacity (Ah) and nominal voltage (V_{Batt}).
2) For the designed DAB converter $V_1 = 600$ V, $V_2 = 380$ V and $V_{Batt} = 320$ V. The values are chosen to facilitate EVCS connection to a 600 V DC microgrid.
3) Compute the value of coupling inductor L_1 using (21).
4) Compute phase shift $\phi = \frac{\pi}{2}(1 - \sqrt{1 - \frac{8f_s L_1 P_0}{n V_1 V_2}})$
5) Compute output capacitor (C_2) and output inductor (L_2) using, $C_2 \frac{dV_2}{dt} = \frac{V_1}{2\pi f_s n L_1} \frac{\phi}{\pi}(1 - \frac{\phi}{\pi}) - \frac{V_2}{R_0}$ and $L_2 \frac{di_0}{dt} = \frac{V_1}{2\pi f_s n L_1} \frac{\phi}{\pi}(1 - \frac{\phi}{\pi})\frac{1}{\omega_s C_2} - I_0(R_0 + \frac{1}{\omega_s C_2})$,
6) Compute the resonance frequency of the output LC filter, $f_r = 1/(2\pi\sqrt{L_2 C_2})$
7) Compute R for the twin-T notch filter using $R = 1/(2\pi C f_r)$ considering C = 0.1 μF.
8) Compute the effective impedance Z_0 using nodal analysis as given in (30).
9) Compute the TF (for CV mode):
$\frac{V_2(s)}{\phi(s)} = \frac{V_1}{2n\pi L_1 f_s}\left(1 - \frac{2\phi}{\pi}\right)\frac{sL_2 + Z_0}{s^2 C_2 L_2 + sC_2 Z_0 + 1}$
10) Compute the TF (for CC mode):
$\frac{i_0(s)}{\phi(s)} = \frac{V_1}{2n\pi L_1 f_s}\left(1 - \frac{2\phi}{\pi}\right)\frac{1}{s^2 C_2 L_2 + sC_2 Z_0 + 1}$
11) Compute the controller parameters by setting appropriate PM and ω_{gc}.

---

this mode lasts until the battery voltage attains an equalization value (V_{eq}). After that, charging enters constant voltage mode. The voltage is kept constant, and the charging current reduces naturally. The flowchart for the battery charging and discharging control is shown in Fig. 9.

$$Z_0 = \frac{16.24 \times 10^{25} s^3 + 29.52 \times 10^{34} s^2 + 27.52 \times 10^{39} s + 6.4 \times 10^{44}}{1.48 \times 10^{28} s^3 + 3.44 \times 10^{33} s^2 + 1.6 \times 10^{38} s + 1.5 \times 10^{42}} \tag{30}$$

$$G_{vd,p} = \frac{6 \times 10^6 s^4 + 10^{12} s^3 + 3 \times 10^{18} s^2 + 3 \times 10^{23} s + 6 \times 10^{27}}{s^5 + 2 \times 10^5 s^4 + 5 \times 10^{11} s^3 + 4.6 \times 10^{16} s^2 + 10^{21} s + 2.5 \times 10^{23}} \tag{31}$$

$$G_{id,p} = \frac{10^{11} s^3 + 3 \times 10^{16} s^2 + 1.5 \times 10^{21} s + 1.4 \times 10^{25}}{s^5 + 2 \times 10^5 s^4 + 5 \times 10^{11} s^3 + 4 \times 10^{16} s^2 + 10^{21} s + 2.5 \times 10^{23}} \tag{32}$$
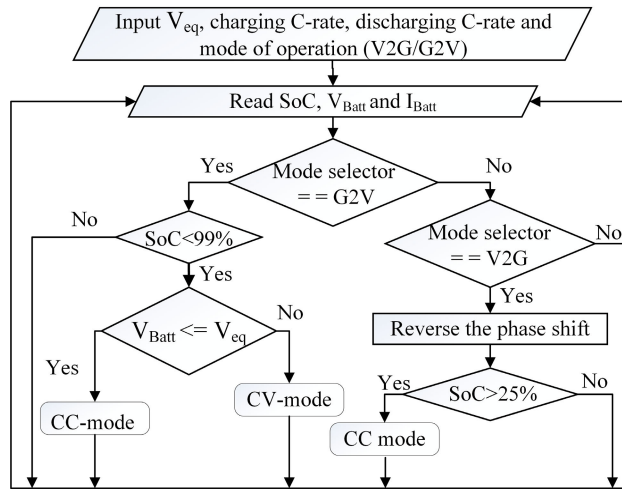
FIGURE 9. Flowchart for the battery charging and discharging control.

IV. RESULTS AND DISCUSSIONS

The Bode plot of the open-loop TF of the system for voltage and current control mode with active damping given by (31) and (32), respectively, is plotted in Fig. 10. The plots indicate that the active damping approach can attenuate the unstable dynamics occurring at the resonance frequency, thus improving the system stability.

For a step input, the system's response for the voltage and current control is plotted in Fig. 11. From the plot, it is inferred that the chosen value of PM and ω_{gc} are optimal. The overshoot is seen eliminated completely, thereby preventing battery degradation.

A notch filter (NF) can be tuned to a particular frequency. However, LC filter parameters can vary, causing resonance frequency to vary. To verify the system robustness, L_2 and C_2 are varied in $\pm10\%$ range. The bode plot in Fig. 12 and Fig. 13 shows no overshoot. Thus, it can be inferred that the proposed system removes unstable dynamics even in the presence of component parameter mismatch/variations.

The designed DAB converter is simulated using Simulink environment, MATLAB R2022a. The MATLAB Simulink block diagram of the proposed model is shown in Fig. 14. The simulation of closed-loop operation is initially carried out by considering a nominal resistive (R) load of 14.44 Ω using current control and voltage control modes separately. The primary (V_p) and secondary (V_s) bridge voltages and the coupling inductor current (I_1) waveform is shown in Fig. 15.

The ZVS of primary and secondary bridge switches is shown in Fig. 16. Fig. 17 shows the DAB converter efficiency curve for varying loads. The efficiency of the designed DAB converter is observed to be 96.1% at the rated load condition.

Subsequently, a battery load is connected. For demonstration, we have chosen a battery with a nominal voltage (V_{Batt}) of 320 V and a capacity of 13 Ah, for which V_{eq} is 372.47 V. The battery is charged at 2C rate to indicate fast charging, and the charge is controlled using the CCCV algorithm. Battery parameter variation viz. SoC, voltage (V_2) and current (I_0) while charging in a closed-loop mode for varying C-rates is
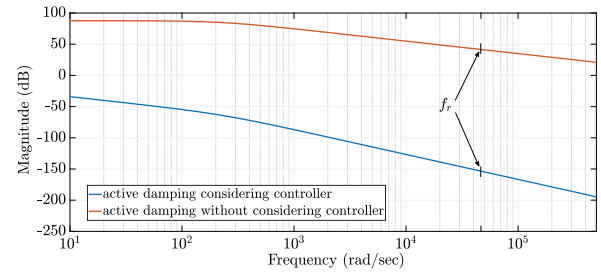
(a)
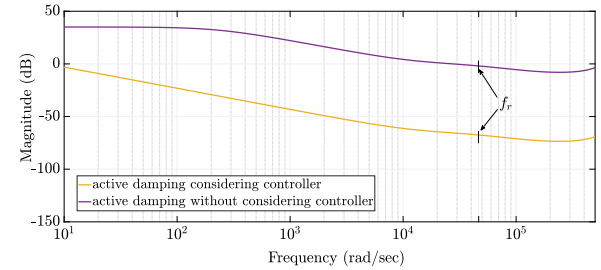
(b)

FIGURE 10. Bode plot of the proposed DAB converter topology in (a) Voltage control mode (b) Current control mode.
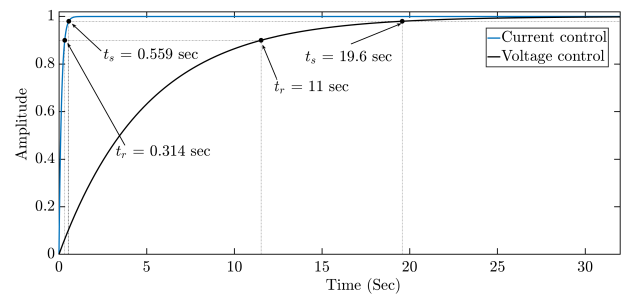

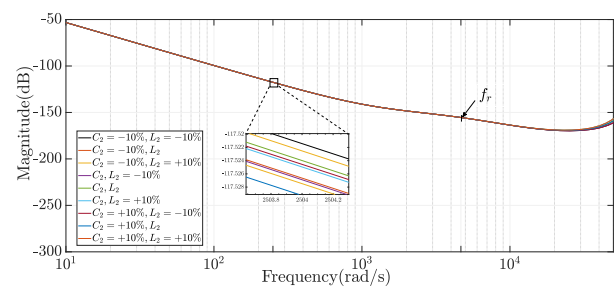**FIGURE 11.** Step response of the proposed closed-loop system.

FIGURE 12. Bode magnitude plot for current control mode considering variations in L_2 and C_2.

shown in Fig. 18. It is observed that the SoC of the battery is gradually increasing from 10% to 66% in response to the change in C-rate.

For the performance evaluation of the developed CCCV controller, the C-rate of the battery was varied from 1C to 2C and again was brought back to 1C by step changing the current drawl (negative direction) from 13 A to 26 A and then reducing back to 13 A as indicated in Fig. 19. It is observed that the phase shift is accordingly increased from
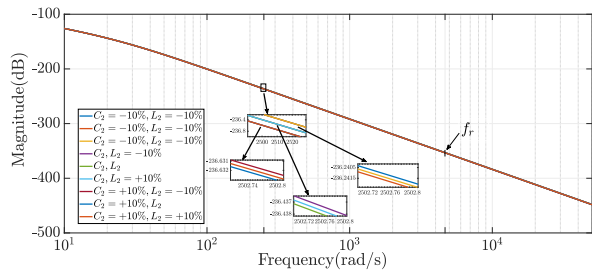
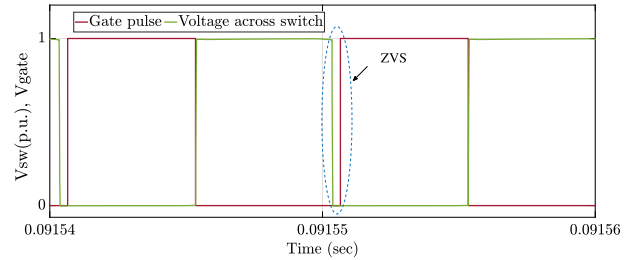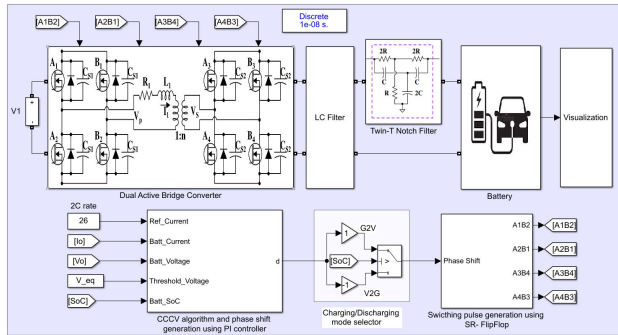**FIGURE 13.** Bode magnitude plot for voltage control mode considering variations in L_2 and C_2.

FIGURE 14. Simulink Model of the proposed DAB converter topology considering twin-T notch filter in cascade.

FIGURE 15. Primary and secondary side bridge voltages and inductor current.

FIGURE 16. Zero Voltage Switching (ZVS) for MOSFET switches.

FIGURE 17. Efficiency curve for various load ratings.

FIGURE 18. Battery parameter variation viz. SoC, voltage (V_2) and current (I_0) while charging at 1C-rate and 2C-rate.

FIGURE 19. Variation in phase-shift with change in C-rate.

2.16° to 23° and then rolled back to 2.16°, thus validating the robustness of the designed controller and theoretical phase-shift computation according to (21). The dynamic response of the proposed model for EV charging at 2C rate is shown in Fig. 20. It is observed that the overshoot in the battery voltage and current during fast charging is reduced drastically. This demonstrates that the proposed approach will aid in reducing battery degradation throughout its life.

Reversing the phase shift between the primary and secondary bridges results in the power flow from the vehicle to the grid. The battery was discharged at 1C rate under CC mode to verify bidirectional operation. The waveform in Fig. 21 depicts a drop in battery SoC from 50% to 25% along with a corresponding decrease in the battery voltage, while keeping current in the dc link, I_s at the constant magnitude. To preserve the longevity, performance, and safety of the battery, the SoC is not permitted to drop below 25% while discharging to the grid.
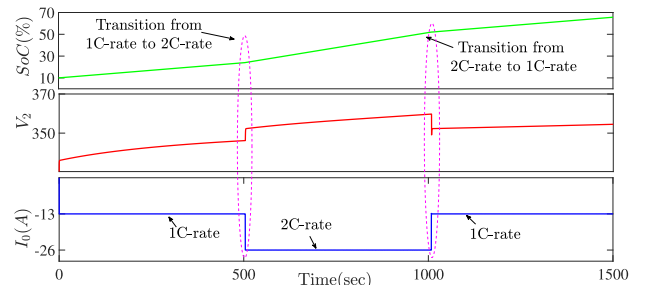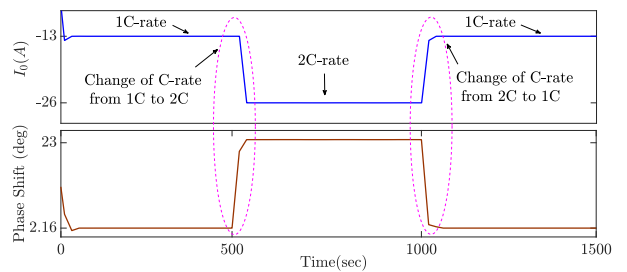
For validating the developed model and the operation of the designed controller for G2V and V2G mode, the system was implemented using a real-time simulator OPAL-RT-4500, as shown in Fig. 22. OPAL-RT(OP)-4500 uses the Field-Programmable-Gate-Array (FPGA) architecture of the OP-4500 and the Xilinx system generator toolbox to realize the system's virtual prototype. The battery was charged for one cycle, going from empty to full. The real-time
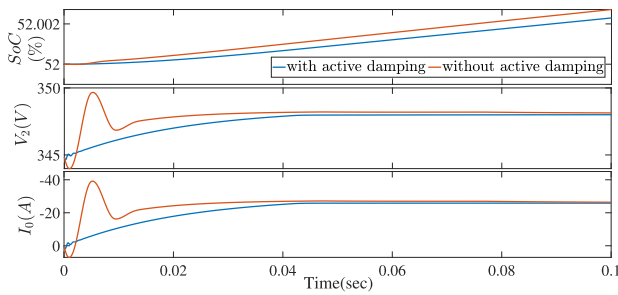
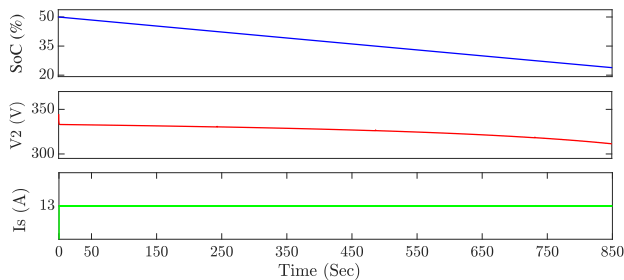**FIGURE 20.** Dynamic response of the proposed model for EV fast charging.

FIGURE 21. Battery parameter variation viz. SoC, voltage (V_2) and dc-link current (I_s) while discharging the battery at 1C-rate.
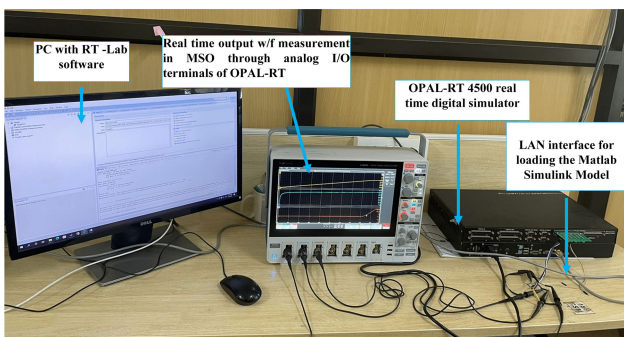

FIGURE 22. Opal-RT hardware test bench setup of the proposed system.
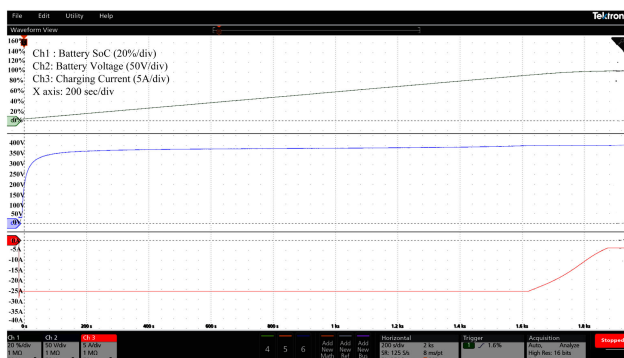

FIGURE 23. OP-4500 implementation results for CCCV battery charging.

simulators result matches with the MATLAB simulation results, as shown in Fig. 23.

V. CONCLUSION

The research work in this paper proposes a topological modification of a Dual Active Bridge (DAB) converter for bidirectional power transfer in a DC microgrid connected fast EV charging station (EVCS). The mathematical modeling of the conventional DAB converter integrated with the LC filter was carried out using GAM and AOCLM techniques, and a small signal model was separately derived for the current and voltage control modes. The stability study carried out using the Bode plot inferred that the proposed system exhibits unstable dynamics or overshoot. In the GAM technique, this overshoot is observed at both the resonant and switching frequencies, but in AOCLM, it is seen only at the resonant frequency. In comparison with the GAM model, AOCLM is simpler, offers higher accuracy and is of 2nd order and hence used for detailed analysis.

Unstable dynamics shorten battery life, especially in fast charging conditions. An active damping approach using a notch filter (NF) was introduced in cascade with DAB to attenuate these unstable dynamics and improve system stability. The proposed active damping method not only achieves resonance damping and loss reduction but also improves the proportional gain of the PID controller, thus satisfying the bandwidth requirement.

Bode analysis is performed to verify the developed system performance for parametric variations in the output LC filter. It is inferred that the proposed converter topology also aids in the improvement of the system's robustness by handling parameter uncertainties. The charge flow to the battery is controlled using the CCCV algorithm. C-rates were varied to test the effectiveness of the controller and the modified topology during battery charging. The results show that the proposed model can effectively control the charging and discharging of the EV battery. In addition, the Zero Voltage Switching (ZVS) technique is implemented to improve efficiency. A Bode diagram with and without NF is plotted to validate the system performance. The efficiency of the designed DAB converter is observed to be 96.1% at the rated load condition.

Dynamic response analysis for EV fast charging infers that the proposed system is essential for optimal performance in fast EVCS. The developed system can have significant practical implications like improved battery health and lifespan, particularly in industries reliant on battery technology. By enabling faster, more efficient, and reliable charging of batteries, the research outcome from this paper contributes to achieving a more sustainable energy future by improving the charging infrastructure and facilitating the integration of renewable energy into the grid.

REFERENCES

[1] S. Kim and F.-S. Kang, "Multifunctional onboard battery charger for plug-in electric vehicles," *IEEE Trans. Ind. Electron.*, vol. 62, no. 6, pp. 3460–3472, Jun. 2015, doi: 10.1109/TIE.2014.2376878.

[2] N. Naik and C. Vyjayanthi, "Optimization of vehicle-to-grid (V2G) services for development of smart electric grid: A review," in *Proc. Int. Conf. Smart Gener. Comput., Commun. Netw.*, Pune, India, Oct. 2021, pp. 1–6, doi: 10.1109/SMARTGENCON51891.2021.9645903.

[3] R. V. S. E. Shravan and C. Vyjayanthi, "Active power filtering using interlinking converter in droop controlled islanded hybrid AC–DC microgrid," *Int. Trans. Electr. Energy Syst.*, vol. 30, no. 5, pp. 1–27, May 2020, doi: 10.1002/2050-7038.12333.

[4] S. Shao, L. Chen, Z. Shan, F. Gao, H. Chen, D. Sha, and T. Dragicevic, "Modeling and advanced control of dual-active-bridge DC–DC converters: A review," *IEEE Trans. Power Electron.*, vol. 37, no. 2, pp. 1524–1547, Feb. 2022, doi: 10.1109/TPEL.2021.3108157.

[5] M. Gopahanal Manjunath, V. Chintamani, and C. Modi, "A real-time hybrid battery state of charge and state of health estimation technique in renewable energy integrated microgrid applications," *Int. J. Emerg. Electr. Power Syst.*, vol. 18, pp. 1–10, May 2022, doi: 10.1515/ijeeps-2021-0434.

[6] L. Zheng, X. Han, Z. An, R. P. Kandula, K. Kandasamy, M. Saeedifard, and D. Divan, "SiC-based 5-kV universal modular soft-switching solid-state transformer (M-S4T) for medium-voltage DC microgrids and distribution grids," *IEEE Trans. Power Electron.*, vol. 36, no. 10, pp. 11326–11343, Oct. 2021, doi: 10.1109/TPEL.2021.3066908.

[7] Q. Xu, N. Vafamand, L. Chen, T. Dragicevic, L. Xie, and F. Blaabjerg, "Review on advanced control technologies for bidirectional DC/DC converters in DC microgrids," *IEEE J. Emerg. Sel. Topics Power Electron.*, vol. 9, no. 2, pp. 1205–1221, Apr. 2021, doi: 10.1109/JESTPE.2020.2978064.

[8] D. Mishra, B. Singh, and B. K. Panigrahi, "Adaptive current control for a bidirectional interleaved EV charger with disturbance rejection," *IEEE Trans. Ind. Appl.*, vol. 57, no. 4, pp. 4080–4090, Jul. 2021, doi: 10.1109/TIA.2021.3074612.

[9] N. Naik and C. Vyjayanthi, "Research on electric vehicle charging system: Key technologies, communication techniques, control strategies and standards," in *Proc. IEEE 2nd Int. Conf. Electr. Power Energy Syst. (ICEPES)*, Bhopal, India, Dec. 2021, pp. 1–6, doi: 10.1109/ICEPES52894.2021.9699496.

[10] S.-A. Amamra and J. Marco, "Vehicle-to-grid aggregator to support power grid and reduce electric vehicle charging cost," *IEEE Access*, vol. 7, pp. 178528–178538, 2019, doi: 10.1109/ACCESS.2019.2958664.

[11] T.-T. Le, H. Jeong, and S. Choi, "A bidirectional three-phase push–pull converter with hybrid PPS-DAPWM switching method for high power and wide voltage range applications," *IEEE Trans. Ind. Electron.*, vol. 68, no. 2, pp. 1322–1331, Feb. 2021, doi: 10.1109/TIE.2020.2969113.

[12] J.-H. Choi, H.-M. Kwon, and J.-Y. Lee, "Design of a 3.3 kW/100 kHz EV charger based on flyback converter with active snubber," *IEEE Trans. Veh. Technol.*, vol. 71, no. 7, pp. 7161–7170, Jul. 2022, doi: 10.1109/TVT.2022.3168625.

[13] T. Jiang, J. Zhang, X. Wu, K. Sheng, and Y. Wang, "A bidirectional LLC resonant converter with automatic forward and backward mode transition," *IEEE Trans. Power Electron.*, vol. 30, no. 2, pp. 757–770, Feb. 2015, doi: 10.1109/TPEL.2014.2307329.

[14] B. Han, J.-S. Lai, and M. Kim, "Dynamic modeling and controller design of dual-mode Cuk inverter in grid-connected PV/TE applications," *IEEE Trans. Power Electron.*, vol. 33, no. 10, pp. 8887–8904, Oct. 2018, doi: 10.1109/TPEL.2017.2779843.

[15] H. Wen, J. Li, H. Shi, Y. Hu, and Y. Yang, "Fault diagnosis and tolerant control of dual-active-bridge converter with triple-phase shift control for bidirectional EV charging systems," *IEEE Trans. Transport. Electrific.*, vol. 7, no. 1, pp. 287–303, Mar. 2021, doi: 10.1109/TTE.2020.3045673.

[16] Y.-C. Jeung and D.-C. Lee, "Voltage and current regulations of bidirectional isolated dual-active-bridge DC–DC converters based on a double-integral sliding mode control," *IEEE Trans. Power Electron.*, vol. 34, no. 7, pp. 6937–6946, Jul. 2019, doi: 10.1109/TPEL.2018.2873834.

[17] Y. Nazih, M. G. Abdel-Moneim, A. A. Aboushady, A. S. Abdel-Khalik, and M. S. Hamad, "A ring-connected dual active bridge based DC–DC multiport converter for EV fast-charging stations," *IEEE Access*, vol. 10, pp. 52052–52066, 2022, doi: 10.1109/ACCESS.2022.3173616.

[18] B. Zhao, Q. Song, J. Li, Y. Wang, and W. Liu, "Modular multilevel high-frequency-link DC transformer based on dual active phase-shift principle for medium-voltage DC power distribution application," *IEEE Trans. Power Electron.*, vol. 32, no. 3, pp. 1779–1791, Mar. 2017, doi: 10.1109/TPEL.2016.2558660.

[19] V. Karthikeyan and R. Gupta, "FRS-DAB converter for elimination of circulation power flow at input and output ends," *IEEE Trans. Ind. Electron.*, vol. 65, no. 3, pp. 2135–2144, Mar. 2018, doi: 10.1109/TIE.2017.2740853.

[20] A. Tuluhong, W. Wang, Y. Li, H. Wang, and L. Xu, "Parasitic parameter extraction and identification method for HFT based on DC–DC converter in EV application," *IEEE J. Emerg. Sel. Topics Power Electron.*, vol. 10, no. 4, pp. 4303–4318, Aug. 2022, doi: 10.1109/JESTPE.2021.3136777.

[21] S. S. Shah and S. Bhattacharya, "A simple unified model for generic operation of dual active bridge converter," *IEEE Trans. Ind. Electron.*, vol. 66, no. 5, pp. 3486–3495, May 2019, doi: 10.1109/TIE.2018.2850012.

[22] N. Naik, C. Vyjayanthi, and C. Modi, "Design, loss analysis and MFA modeling of DAB-based fast charger for bidirectional grid to EV power transfer," in *Proc. Int. Conf. Advancement Technol. (ICONAT)*, Goa, India, Jan. 2023, pp. 1–7, doi: 10.1109/ICONAT57137.2023.10080578.

[23] S. Mukherjee, A. Kumar, and S. Chakraborty, "Comparison of DAB and LLC DC–DC converters in high-step-down fixed-conversion-ratio (DCX) applications," *IEEE Trans. Power Electron.*, vol. 36, no. 4, pp. 4383–4398, Apr. 2021, doi: 10.1109/TPEL.2020.3019796.

[24] Q. Ye, R. Mo, and H. Li, "Impedance modeling and DC bus voltage stability assessment of a solid-state-transformer-enabled hybrid AC–DC grid considering bidirectional power flow," *IEEE Trans. Ind. Electron.*, vol. 67, no. 8, pp. 6531–6540, Aug. 2020, doi: 10.1109/TIE.2019.2937039.

[25] E. S. Lee, J. H. Park, M. Y. Kim, and J. S. Lee, "High efficiency integrated transformer design in DAB converters for solid-state transformers," *IEEE Trans. Veh. Technol.*, vol. 71, no. 7, pp. 7147–7160, Jul. 2022, doi: 10.1109/TVT.2022.3168561.

[26] M. Wang, S. Pan, X. Zha, J. Gong, W. Lin, J. Gao, and Q. Deng, "Hybrid control strategy for an integrated DAB–LLC–DCX DC–DC converter to achieve full-power-range zero-voltage switching," *IEEE Trans. Power Electron.*, vol. 36, no. 12, pp. 14383–14397, Dec. 2021, doi: 10.1109/TPEL.2021.3086633.

[27] L. Gong, X. Jin, J. Xu, Z. Deng, H. Li, T. B. Soeiro, and Y. Wang, "A dynamic ZVS-guaranteed and seamless-mode-transition modulation scheme for the DAB converter that maximizes the ZVS range and lowers the inductor RMS current," *IEEE Trans. Power Electron.*, vol. 37, no. 11, pp. 13119–13134, Nov. 2022, doi: 10.1109/TPEL.2022.3180759.

[28] L. Shu, W. Chen, M. Shi, R. Liu, S. Gao, and F. Deng, "Improved control strategy of triple-voltage three-phase DAB (T^2-DAB) converter for current stress and zero-voltage-switching optimization," *IEEE J. Emerg. Sel. Topics Power Electron.*, vol. 10, no. 1, pp. 773–784, Feb. 2022, doi: 10.1109/JESTPE.2021.3060477.

[29] E. L. Carvalho, C. A. Felipe, L. V. Bellinaso, C. M. D. O. Stein, R. Cardoso, and L. Michels, "Asymmetrical-PWM DAB converter with extended ZVS/ZCS range and reduced circulating current for ESS applications," *IEEE Trans. Power Electron.*, vol. 36, no. 11, pp. 12990–13001, Nov. 2021, doi: 10.1109/TPEL.2021.3078734.

[30] G. Waltrich, M. A. M. Hendrix, and J. L. Duarte, "Three-phase bidirectional DC/DC converter with six inverter legs in parallel for EV applications," *IEEE Trans. Ind. Electron.*, vol. 63, no. 3, pp. 1372–1384, Mar. 2016, doi: 10.1109/TIE.2015.2494001.

[31] S. A. Assadi, H. Matsumoto, M. Moshirvaziri, M. Nasr, M. S. Zaman, and O. Trescases, "Active saturation mitigation in high-density dual-active-bridge DC–DC converter for on-board EV charger applications," *IEEE Trans. Power Electron.*, vol. 35, no. 4, pp. 4376–4387, Apr. 2020, doi: 10.1109/TPEL.2019.2939301.

[32] Y. Park, S. Chakraborty, and A. Khaligh, "DAB converter for EV onboard chargers using bare-die SiC MOSFETs and leakage-integrated planar transformer," *IEEE Trans. Transport. Electrific.*, vol. 8, no. 1, pp. 209–224, Mar. 2022, doi: 10.1109/TTE.2021.3121172.

[33] D. Das, S. Mishra, and B. Singh, "Design architecture for continuous-time control of dual active bridge converter," *IEEE J. Emerg. Sel. Topics Power Electron.*, vol. 9, no. 3, pp. 3287–3295, Jun. 2021, doi: 10.1109/JESTPE.2020.3000340.

[34] P. F. S. Costa, P. H. B. Löbler, L. Roggia, and L. Schuch, "Modeling and control of DAB converter applied to batteries charging," *IEEE Trans. Energy Convers.*, vol. 37, no. 1, pp. 175–184, Mar. 2022, doi: 10.1109/TEC.2021.3082468.

[35] V. M. Iyer, S. Gulur, and S. Bhattacharya, "Small-signal stability assessment and active stabilization of a bidirectional battery charger," *IEEE Trans. Ind. Appl.*, vol. 55, no. 1, pp. 563–574, Jan. 2019, doi: 10.1109/TIA.2018.2871101.

[36] D. Chen, J. Deng, W. Wang, and Z. Wang, "A dual-transformer-based hybrid dual active bridge converter for plug-in electric vehicle charging to cope with wide load voltages," *IEEE Trans. Ind. Electron.*, vol. 70, no. 2, pp. 1444–1454, Feb. 2023, doi: 10.1109/TIE.2022.3158013.

[37] N. J. M. Mary, S. Sathyan, and H. M. Suryawanshi, "A three-level resonant DAB converter featuring minimized circulating losses for EV battery charging," *IEEE Trans. Ind. Electron.*, vol. 70, no. 8, pp. 7879–7890, Aug. 2023, doi: 10.1109/TIE.2023.3234135.

[38] S.-T. Wu and B.-Y. Yang, "Design and implementation of an isolated bidirectional phase-shift full-bridge converter with high transformation ratio," *IEEE Access*, vol. 11, pp. 17945–17955, 2023, doi: 10.1109/ACCESS.2023.3246261.

[39] S. Chaurasiya and B. Singh, "A bidirectional fast EV charger for wide voltage range using three-level DAB based on current and voltage stress optimization," *IEEE Trans. Transport. Electrific.*, vol. 9, no. 1, pp. 1330–1340, Mar. 2023, doi: 10.1109/TTE.2022.3201979.

[40] O. Zayed, A. Elezab, A. Abuelnaga, and M. Narimani, "A dual-active bridge converter with a wide output voltage range (200–1000 V) for ultra-fast DC-connected EV charging stations," *IEEE Trans. Transport. Electrific.*, early access, Dec. 26, 2022, doi: 10.1109/TTE.2022.3232560.

[41] J. Tian, F. Wang, F. Zhuo, and H. Deng, "Research on multiple duty modulation scheme in dual-active-bridge-based energy storage system," *IEEE J. Emerg. Sel. Topics Power Electron.*, vol. 11, no. 3, pp. 3562–3573, Jun. 2023, doi: 10.1109/JESTPE.2023.3255247.

[42] M. M. Haque, P. Wolfs, S. Alahakoon, B. C. P. Sturmberg, M. Nadarajah, and F. Zare, "DAB converter with Q capability for BESS/EV applications to allow V2H/V2G services," *IEEE Trans. Ind. Appl.*, vol. 58, no. 1, pp. 468–480, Jan. 2022, doi: 10.1109/TIA.2021.3123139.

[43] J. Tian, F. Wang, F. Zhuo, X. Cui, and D. Yang, "An optimal primary-side duty modulation scheme with minimum peak-to-peak current stress for DAB-based EV applications," *IEEE Trans. Ind. Electron.*, vol. 70, no. 7, pp. 6798–6808, Jul. 2023, doi: 10.1109/TIE.2022.3206698.

[44] V. A. Caliskan, O. C. Verghese, and A. M. Stankovic, "Multifrequency averaging of DC/DC converters," *IEEE Trans. Power Electron.*, vol. 14, no. 1, pp. 124–133, Jan. 1999, doi: 10.1109/63.737600.

[45] S. R. Sanders, J. M. Noworolski, X. Z. Liu, and G. C. Verghese, "Generalized averaging method for power conversion circuits," *IEEE Trans. Power Electron.*, vol. 6, no. 2, pp. 251–259, Apr. 1991, doi: 10.1109/63.76811.

[46] H. Qin and J. W. Kimball, "Generalized average modeling of dual active bridge DC–DC converter," *IEEE Trans. Power Electron.*, vol. 27, no. 4, pp. 2078–2084, Apr. 2012, doi: 10.1109/TPEL.2011.2165734.

[47] J. A. Mueller and J. W. Kimball, "An improved generalized average model of DC–DC dual active bridge converters," *IEEE Trans. Power Electron.*, vol. 33, no. 11, pp. 9975–9988, Nov. 2018, doi: 10.1109/TPEL.2018.2797966.

[48] J. Dannehl, M. Liserre, and F. W. Fuchs, "Filter-based active damping of voltage source converters with *LCL* filter," *IEEE Trans. Ind. Electron.*, vol. 58, no. 8, pp. 3623–3633, Aug. 2011, doi: 10.1109/TIE.2010.2081952.

[49] M. Ye, H. Gong, R. Xiong, and H. Mu, "Research on the battery charging strategy with charging and temperature rising control awareness," *IEEE Access*, vol. 6, pp. 64193–64201, 2018, doi: 10.1109/ACCESS.2018.2876359.

C. VYJAYANTHI (Member, IEEE) received the M.Tech. degree in power systems from Anna University, India, in 2005, and the Ph.D. degree in power systems from the Indian Institute of Science, Bengaluru, India, in 2011. She has been an Associate Professor with the Department of Electrical and Electronics Engineering, National Institute of Technology Goa (NIT Goa), India, since 2014. She has authored or coauthored many articles in reputed journals and international conference proceedings. She holds two research-funded projects, such as Development of a Multipurpose Intelligent Controller for a Nano Grid Operation from the Ministry of New and Renewable Energy, India; and Development of Coordination Control Schemes for Hybrid AC/DC Microgrids for a Stable and Reliable System Operation, from Science and Engineering Research Board (SERB), Department of Science and Technology (DST), India. She is an active member of the Blockchain Research Laboratory, NIT Goa. She is a Co-Investigator of research funded project titled "Developing Smart Controller for Optimum Utilization of Energy and Trustworthy Management in a Micro Grid Environment" with funding support under IMPacting Research INnovation and Technlogy-2 C1 (IMPRINT-2 C1) by Science and Engineering Research Board (SERB). Her research interests include restructured power systems; planning, operation, and control of power systems; electric arc furnace operations; smart electric grids; flexible ac transmission systems; ac/dc microgrids; and cyber security.

CHIRAG MODI (Senior Member, IEEE) received the M.Tech. and Ph.D. degrees in computer engineering from the National Institute of Technology Surat, Gujarat, India, in 2010 and 2014, respectively. He has been an Assistant Professor of computer science and engineering with the National Institute of Technology Goa, Goa, India, since 2014. He holds research funded project titled "Developing Smart Controller for Optimum Utilization of Energy and Trustworthy Management in a Micro Grid Environment" with funding support under IMPacting Research INnovation and Technlogy-2 C1 (IMPRINT-2 C1) by the Science and Engineering Research Board (SERB), Department of Science and Technology, Government of India. He has authored or coauthored many articles in reputed journals and international conference proceedings. His research interests include information security and privacy, cryptography, cloud security, network security, intrusion detection, and privacy preserving data mining. He was a recipient of the Young Scientist Award in Specialization of Cloud Computing from VIFRA, Chennai, India, in 2015; and the Best Review Paper Award from *Journal of Network and Computer Applications* (JNCA), Elsevier, San Diego, USA, in 2015. He was also a recipient of the first position in the National level workshop and competition on Ethical Hacking, conducted by Wegillent Inc., in association with the Indian Institute of Technology Roorkee, Uttarakhand, India, and the National Institute of Technology Surat, in 2013.

• • •

NIVEDITA NAIK received the M.E. degree in power electronics and drives from AISSMS COE, SP Pune University, in 2015. She is a Research Scholar with the Department of Electrical and Electronics Engineering, National Institute of Technology Goa (NIT Goa), Ponda, Goa. Her research interests include smart grids, power electronics, electric vehicles, optimization algorithm development, MPPT, and grid integrated PV, wind, and battery system control.